Journal of Power Sources 268 (2014) 255–260

Contents lists available at ScienceDirect

Journal of Power Sources

journal homepage: www.elsevier.com/locate/jpowsour

Mesoporous Pt–Co oxygen reduction reaction (ORR) catalysts for low temperature proton exchange membrane fuel cell synthesized by alternating sputtering

Gustav Sievers [a, *], Steffen Mueller [a], Antje Quade [a], Florian Steffen [b], Sven Jakubith [b], Angela Kruth [a], Volker Brueser [a]

[a] Institute for Plasma Science and Technology, Felix-Hausdorff-Str. 2, 17489 Greifswald, Germany
[b] EKPRO GmbH, Gardeschuetzenweg 7, 12203, Berlin

HIGHLIGHTS

- Mesoporous Pt–Co catalysts showed enhanced ORR activity for PEMFC.
- The best Co layer thickness was determined to be 2 nm.
- The kinetic current could be increased by a factor of 16.
- Pt mass activity was optimized at a layer thickness of 30.5 nm.
- Mass activity in the fuel cell could be increased by a factor of 7.

GRAPHICAL ABSTRACT

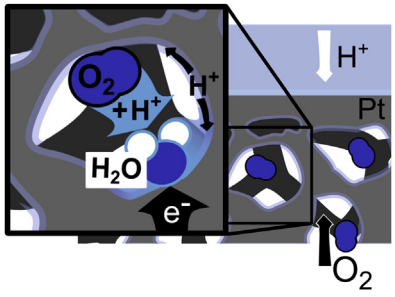

ARTICLE INFO

Article history:
Received 3 February 2014
Received in revised form
2 June 2014
Accepted 3 June 2014
Available online 16 June 2014

Keywords:
Proton exchange membrane fuel cell
Platinum
Cobalt
Oxygen reduction reaction
Mesoporous
Rotating disk electrode

ABSTRACT

Mesoporous catalysts with enhanced oxygen reduction reaction (ORR) activity for PEM fuel cells are synthesized by alternating sputtering of Pt and Co onto gas diffusion layers with microporous layers. Co is acting as a template for synthesis of a porous Pt nanostructure. For such proposed Pt–Co catalysts the kinetic current in the ORR was found to be increased by a factor of up to 16 and the mass specific current in PEM single cells by a factor of up to 7. Co was found to be deposited at the grain boundary of the Pt layer and dissolves under acidic conditions resulting in a mesoporous Pt catalyst which is advantageous for gas diffusion catalysts. Microstructural and compositional parameters were optimised in order to obtain a high kinetic current and lower onset potential for the ORR. The most favourable Co layer thickness was determined to be 2 nm. The optimal Pt–Co catalyst can be synthesized by continuously varying the Pt layer thickness. The highest Pt mass activity was found at a layer thickness of 30.5 nm. Catalysts were characterised by SEM, EDX, electrochemical half cell and PEM single cell tests.

1. Introduction

A key issue in the development and economic enforceability of Polymer Electrolyte Membrane Fuel Cells (PEMFC) is to develop an efficient and affordable catalyst system, therefore the Pt loading has to be reduced significantly. Especially slow kinetics of the oxygen reduction reaction (ORR) at the cathode side and low Pt utilisation due to inhibited mass transfer have to be improved. This goal can be achieved either by reducing the activation energy of the ORR or by a more efficient use of Pt in the catalyst layer (CL).

* Corresponding author. Tel.: +49 3834 554 3863; fax: +49 3834 554 301.
E-mail address: gustav.sievers@inp-greifswald.de (G. Sievers).

http://dx.doi.org/10.1016/j.jpowsour.2014.06.013
0378-7753/

Table 1
Synthesis parameters for Pt–Co catalysts on glassy carbon electrodes for half cell testing.

	catalyst number	Pt per layer μg cm^{-2} nm^{-1}	Co per layer μg cm^{-2} nm^{-1}	Iteration *n*	Total Pt μg cm^{-2}	Height nm
ORR	$PtCo_n$	2.0/1.7	2.7/3	1–10	n * 2	n * 4.7
	$PtCo_A$	10.2/84	1.8/2	2	20.3	20.8
	$PtCo_B$	6.8/5.6	1.8/2	3	20.3	22.2
	$PtCo_C$	4.1/3.4	1.8/2	5	20.3	27.0
	$PtCo_D$	Catalyst with increasing Pt content, Pt loading by layer per cm^{-2}: 0.7 μg (0.6 nm)/1.4 μg (1.1 nm)/ 2.7 μg (2.2 nm)/5.4 μg (4.5 nm)/10.2 μg (8.4 nm). Each layer is interrupted by 8.1 μg/9 nm Co				
	$PtCo_E$	Catalyst with decreasing Pt content, Pt loading by layer per cm^{-2}: 10.2 μg (8.4 nm)/5.4 μg (4.5 nm)/ 2.7 μg (2.2 nm)/1.4 μg (1.1 nm)/0.7 μg (0.6 nm). Each layer is interrupted by 8.1 μg/9 nm Co				

The activation energy can be decreased using bimetallic alloys containing transition metals such as Co, Ni or Fe which were reported to enhance the specific activity for the oxygen reduction reaction by a factor of 2–10 [1–6]. Hence the amount of Pt can be reduced significantly [7]. Besides $Pt_3Ni(111)$ and $Pt(111)Co_3$, which are difficult to produce on a large scale, Pt_3Co showed the highest specific activity enhancement of the bimetallic Pt–Co [8,9]. There are several reasons for the enhancement: Firstly Co is leached out in acidic conditions resulting in a roughened surface. In the presence of some remaining Co a different d-band configuration of Pt–Co is obtained as compared to pure Pt increasing the ORR activity due to a smaller O binding energy [10]. Furthermore geometric structure, lattice constraints, particle size, real surface area, wettability and redox type processes are influenced by the presence of Co [11]. Pt–Co nanoparticles are found to be unstable under PEMFC operating conditions, however, an enrichment of Pt in the outer shell and dissolution of Co in the inner core will result in a relative stable hollow Pt sphere [12].

Another highly important aspect is the utilization of the catalyst in the CL. Due to the fact that the efficiency of Pt is influenced by the thickness of the catalyst layer [13] and the particle size effect [14], research efforts are shifting towards the synthesis of extended nanostructured catalysts [15]. The most known extended catalyst is a nanostructured thin film (NSTF) by Debe et al. which was reported to reach a specific activity up to 20 times higher compared to conventional Pt/C catalysts [16]. In these catalysts H^+ conductivity is enabled by surface migration of hydronium ions over the Pt–OH covered surface or by H_2O diffusion into the pores considering the Grotthuss mechanism [16]. As well as the enhancement of the specific activity it is crucial to avoid the corroding carbon support. Following the hypothesis, we expect that the long-term stability of the catalyst can be significantly increased by avoiding a carbon support. Furthermore the use of Nafion as H^+ conductor in the electrode may be problematic. Nafion limits the ORR through anion adsorption and hindrance of oxygen diffusion. Few studies concerned with supportless extended surface catalysts were carried out up to this moment: mesostructured thin films [17,18], aerogels [19], Pt nanotubes [20], simultaneous sputtering [21,6,22] or alternating sputtering [23,24].

The mesoporous CL used in this work is produced by a dual-magnetron sputtering process using Pt and Co targets. Up to now, such an alternating sputtering process for deposition of Pt and Co on the MPL was not investigated in detail. The advantage that the resulting mesoporous structure may have in electrode applications needs to be further emphasized. Therefore we investigated the influence of Co and Pt layer thickness and the structure of the Pt–Co layer assembly on the electrode properties by analysis of the ORR activity and PEMFC performance as well as microstructure and elemental composition by RDE, PEM single fuel cell, SEM, EDX and XRD.

2. Experimental part

2.1. Synthesis of Pt/Co catalyst layer

Pt–Co layers were synthesized through an alternating sputtering process of Pt and Co. The reactor chamber was evacuated to a base pressure of $5 \cdot 10^{-3}$ Pa. An argon plasma was ignited in the chamber at a working pressure of 5 Pa. Two magnetrons were equipped with planar targets of Co (99,9%, Mateck GmbH, Germany) and Pt (99,95%, Junker Edelmetalle, Germany). They were located on the superior part of the recipient. The RF generators (Advanced Energy) had a driving frequency of 13,56 MHz. The recipient (Neoplas GmbH, Germany) was configurated in that way that the substrate holder is turned automatically towards the respective magnetron with the sputtering being initiated when the sample is in position below the magnetron. Pt–Co catalysts are synthesized by alternatingly turning the subtrate into positions below the Co or the Pt target and deposition times and magnetron powers were varied. The catalysts were deposited onto the microporous layer (MPL) of the gas diffusive layer (GDL) for subsequent PEMFC testing or onto a glassy carbon electrode to be able to carry out RDE measurements. The nominal thickness was measured by using a Dektak 3ST profilometer on samples deposited onto flat glass. However, the real thickness of the deposited layers is expected to vary depending on substrate roughness. The real thickness of the Pt–Co layers on the MPL is likely to be smaller than its nominal thickness because the real surface area is higher than the geometric surface area. When Pt–Co is deposited on glassy carbon, the real thickness is comparable to the nominal thickness because the roughness is negligible. Synthesis procedures for each catalyst sample are summarized with regard to the electrochemical half cell tests in Table 1 and the PEM single fuel cell tests in Table 2. Pt–Co catalysts for electrochemical half cell tests were synthesized by successive deposition of Pt and Co ($PtCo_n$, Fig. 3), variation of the Co layer thickness with constant Pt loading (Fig. 4) and variation of the Pt–Co assembly with a constant Pt loading (Fig. 5). Co was sputtered always initially. A schematic illustration of the synthesis procedure is shown in Fig. 1.

Table 2
Synthesis parameters for Pt–Co catalysts on GDL/MPL for single fuel cell testing.

	Catalyst number	Pt per layer μg cm^{-2} nm^{-1}	Co per layer μg cm^{-2} nm^{-1}	Iteration cathode	Total Pt μg cm^{-2}
PEMFC	$PtCo_{F1}$	20/17	1.8/2	4	120
	$PtCo_{F2}$	20/17	1.8/2	2	60
	$PtCo_{F3}$	10/8.4	1.8/2	4	60
	$PtCo_{F4}$	4/3.4	1.8/2	10	60
	Pt pure	–	–	–	700

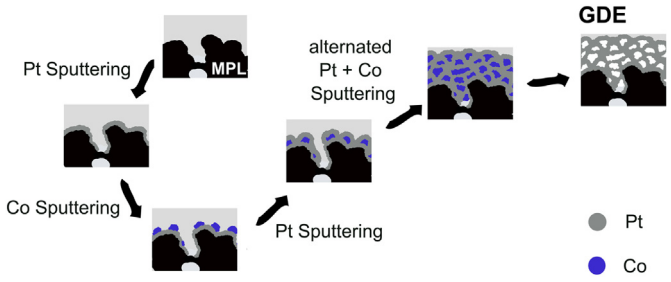

Fig. 1. Synthesis of a mesostructured Pt–Co catalyst template by alternating sputtering of Pt and Co followed by a dissolution of Co in the electrochemical cell results in a highly active mesoporous Pt catalyst.

2.2. PEM single fuel cell

The electrodes of the MEA in the single fuel cell had a geometric surface area of 25 cm^2. The Pt loading of the cathode was always twice of the Pt loading of the anode, see Table 2. As membrane material Nafion NM 212 was used. The membrane was conditioned in 3% H_2O_2 (1 h), in double distilled H_2O (1 h), 3 %H_2SO_4 (1 h) and again in double distilled H_2O (1 h) at 333 K before MEA assembly. The membrane electrode assembly (MEA) was hot pressed between two heated aluminium cubes at 423 K with bar spacers to 90% of the initial thickness. The single cell test system was a Quickconnect (balticFuelCells, Germany) that was equipped with a constant contact pressure unit in order to control the pressure achieving a better reproducibility of MEA testing. The test station was controlled with LabVIEW and was programmed and designed by EKPRO GmbH (Germany). The cell was operated at 346 K with approximate 100% humidity in the cathode stream ($\lambda = 10$) and dry anode stream ($\lambda = 1$) in dead-end mode with humidification of the membrane being provided from the cathode by diffusion. [25] As a precaution to avoid any excess water that might be present, air purges were performed intermittently. The MEA was conditioned by a special method to activate the MEA unit. Non-steady-state polarisation curves were obtained by fast potential sweeping with 100 mV s^{-1} from 100 mV to the open circuit potential (OCV) [26]. Air and H_2 purges were performed intermittently to remove process water from the cathode and anode. The water at the anode is due to crossdiffusion through the membrane. As reference, we used a commercial available screenprinted Pt/C MEA (balticFuelCells).

2.3. Rotating disc electrode

The RDE measurements were carried out by using a rotator by PINE (USA) and a bipotentiostat by Metrohm Autolab (Germany). The Pt–Co layers were deposited directly onto the glassy carbon electrodes during the physical vapour deposition process. The Pt

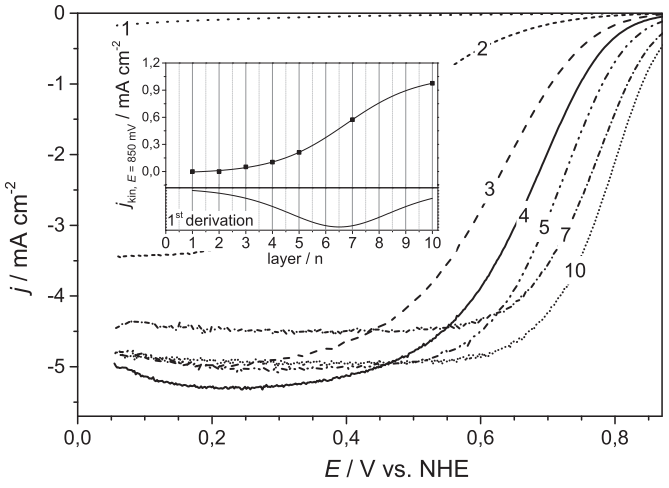

Fig. 3. LSV of successive deposited Pt–Co layers in 0.5 M H_2SO_4 in a O_2 saturated solution vs. NHE, $\omega = 1600$ RPM, $T = 333$ K, $\nu = 5$ mV s^{-1}, inset: Kinetic current at 850 mV vs. NHE for each deposited Pt–Co layers and the first derivation of the Boltzmann fit for determination of the Maxima, for synthesis procedure see Table 1 $PtCo_n$.

electrode (20.3 μg cm^{-2}) was prepared by sputtering from a single Pt target onto glassy carbon. The glassy carbon electrodes had a diameter of 5 mm. The parameters of the electrochemical tests have been chosen according to the work of Gasteiger et al. [27]. However, we used 0.5 M H_2SO_4 (Sigma–Aldrich Germany, TraceSelect®) and ultrapure H_2O (18.2 MΩ, Milli-Q-Integral 3) at 333 K, with rotation speeds between 400 and 2500 RPM. All glassware was thoroughly cleaned before measurements with piranha solutions and ultrapure water. The three electrode setup was equipped with a Ag/AgCl (3.5 M KCl) reference electrode and a Pt wire as counter electrode. When the typical cyclic voltammogram from −0.3 V to 1.3 V vs. Ag/AgCl of Pt was free of contamination, linear sweep voltammetry from 1 V to 0.05 V vs. NHE for analysis of the ORR was carried out with a potential sweep rate of 5 mV s^{-1}. The kinetic current j_{kin} is calculated by

$$j_{kin} = \frac{j_{dif} \times j}{j_{dif} - j} \quad (1)$$

where j_{dif} is the diffusion limited current measured over the entire potential range between 500 mV and 100 mV vs. NHE.

2.4. SEM and GIXRD

The SEM (JSM 7500F, JEOL) employs a field-emission gun, a semi-in-lens conical objective lens and a secondary electron in-lens detector for high-resolution and high-quality image observation of

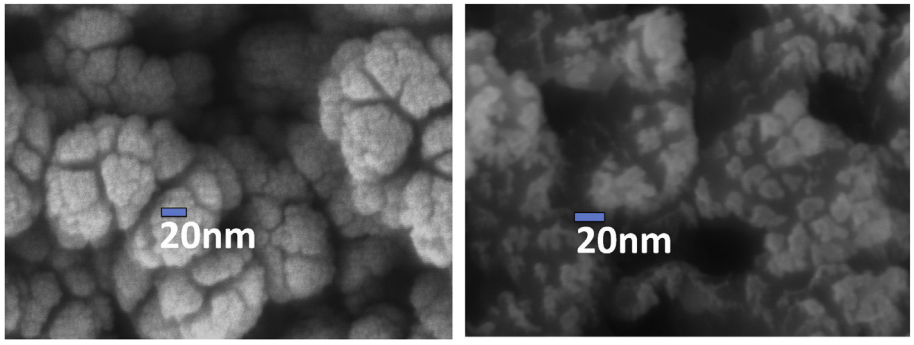

Fig. 2. SEM picture of Pt–Co with Pt as last deposition step (left) and Co as last deposition step (right) deposited on a MPL.

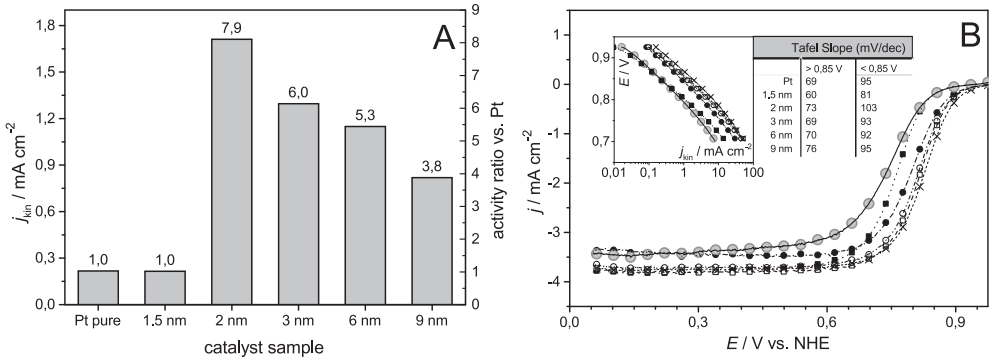

Fig. 4. ORR analysis of Pt–Co layers with different Co thickness. A Kinetic current at 850 mV vs. NHE. B: Hydrodynamic voltammograms of Pt (–●–) and Pt–Co catalysts interrupted by 1.5 nm (·-■-·), 2 nm (·-×-·), 3 nm (–□–), 6 nm (--○--) and 9 nm (--●--) Co layers investigated at 850 mV vs. NHE in 0.5 M H_2SO_4 in a O_2 saturated solution (ω = 900 RPM, T = 333 K, ν = 5 mV s^{-1}) with different Co loadings but the same Pt loading. In the inset of B the data is illustrated as Tafel plot. The nominal thickness of the Co layer is given as sample name. All samples are prepared as Pt–Co_C (Table 1) varying the Co layer thickness.

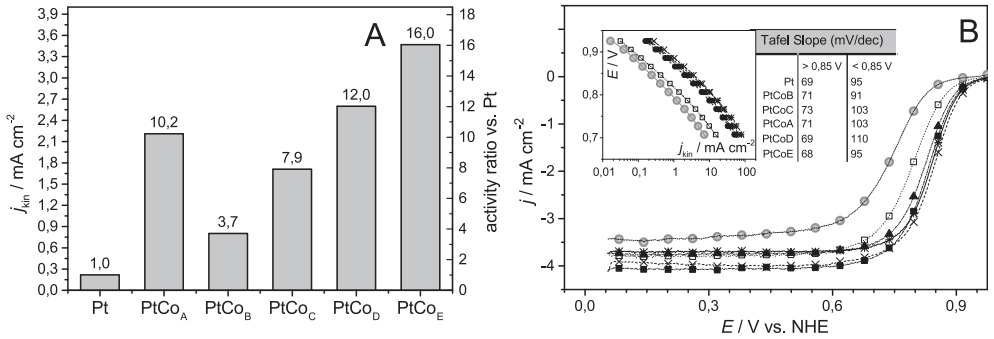

Fig. 5. ORR analysis of different Pt–Co layer assemblies. A Kinetic current at 850 mV vs. NHE; B: Hydrodynamic voltammograms of Pt (–●–), $PtCo_A$ (·-■-·), $PtCo_B$ (–□–), $PtCo_C$ (--●--), $PtCo_D$ (·-×-·), $PtCo_E$(--●--) investigated at 850 mV vs. NHE in 0.5 M H_2SO_4 in a O_2 saturated solution (ω = 900 RPM, T = 333 K, ν = 5 mV s^{-1}) with different synthesis procedures, but the same Pt loading. In the inset of B the data is illustrated as Tafel plot. The synthesis procedure is described in Table 1.

structural features of the deposited films at a maximum specified resolution of 1.0 nm at 15 keV. The technique enables imaging of the surface without any preparative coatings. Phase identity and crystallinity were investigated by the means of a Bruker D8 Advance Diffractometer with Grazing Incident X-ray diffraction (GIXRD) measurements performed at an incident angle of $\omega = 0.5°$ over a range of 2θ of 20°–80° with a step width of 0.02° and 5 s per step.

3. Results and discussions

3.1. SEM, EDX and GIXRD

SEM analysis (Fig. 2 left) shows the nanostructure comprising of Pt–Co. Apparently the growth mechanism of Pt on the substrate resulted in Pt nanoparticles smaller than 10 nm and an uniform film. As the SEM images suggest Co was growing on top of Pt along side the edges and grain boundaries of Pt. This indicates a non-uniform growth mechanism. This growth mechanism is considered as most advantageous with regard to the catalyst properties. Pt is deposited as a discrete film and Co is deposited as nucleation islands. According to XRD no crystalline structures of Co were detected. EDX measurements confirmed that an electrochemical treatment of the catalyst in 0.5 M sulphuric acid largely removed Co from the catalyst layer leaving behind a Pt mesostructure with possibly traces of Co.

3.2. Electrochemical activity in the ORR and in the fuel cell

3.2.1. ORR activity of successive deposited Pt–Co layers

Pt–Co layers are deposited layer by layer on the glassy carbon and the electrocatalytic activity was measured for each new Pt–Co layer deposited on the glassy carbon. Each catalyst was prepared completely new. The oxygen reduction current in relation to the successive deposited Pt–Co layers is illustrated in Fig. 3. The typical LSV with a comparable diffusion controlled current is achieved with 3 Pt–Co layers adding to a total nominal layer thickness of 14.1 nm corresponding to 5.1 nm Pt (6 μg cm^{-2} Pt) which is not seen with only 1 or 2 Pt–Co layers, see Fig. 3. It could be that a minimum of Pt is needed in order to reach a sufficient specific current and therefore a good mass activity. This is in agreement with the studies carried out by O'Hayre et al. [28] where a thickness between 5 and 10 nm gave the best performance with sputtered Pt on Nafion membranes tested in a single cell and Cha and Lee who examined that the best mass activity is found at a sputtered Pt layer thickness of 5 nm, when compared to 1 nm, 10 nm and 20 nm [29]. The decrease in Pt utilisation with an ever thicker sputtered Pt layer is caused due to several reasons, most important of which are gas diffusion and H^+ transport [30,16]. An interesting fact is the lower catalyst utilisation when the thickness is below 5 nm. This corresponds to the optimum of the size–dependent activity of Pt nanoparticles where a maximum of the mass activity is measured between 3 and 5 nm [31]. The derivation of the current gain of each layer has the maximum situated between 6 and 7 layers (Fig. 3 inset). Therefore it can be sustained as a novelty that the best Pt usage is reached at a total layer thickness of 30.5 nm (only 11 nm Pt) and a Pt loading of 13 μg cm^{-2}. Hence, further deposition of Pt improves the catalyst activity less than the beforehand deposited Pt.

3.2.2. ORR activity of Pt–Co layers with different Co thickness

By changing the thickness of the Co layer inside the catalyst it is possible to gain information about the optimal Pt–Co configuration

(Fig. 4). The kinetic current is compared at a potential of 850 mV vs. NHE rotated with 900 RPM. All samples have an equal Pt loading and are synthesized as $PtCo_C$ with varying Co layer thickness. The Pt–Co catalysts contain 5 layers of Co, each leading to a thickness of 1.5, 2, 3, 6 or 9 nm (Table 1). The kinetic current of pure Pt is comparable to the lowest Co loading −1.5 nm. With this small Co loading there is no difference in the detected kinetic current. Increasing the Co load only slightly to 2 nm, j_{kin} rises by a factor of 6. Co layers having a thickness greater than 2 nm, j_{kin} is still higher than pure Pt, but the maximum enhancement which is found at a Co layer thickness of 2 nm is unreached. The positive influence of Co on Pt is limited by the thickness of the dividing Co layers. If the dissolution of the Co is complete, the mass transfer seems not to be a limiting step. However, it is likely that, in some cases, the Co dissolution is incomplete. Then Co may inhibit the active centers of Pt and lead to a somehow decreased ORR activity. The Tafel slopes of Pt and Pt–Co plotted with the diffusion-corrected kinetic currents are in the same order.

3.2.3. ORR activity of different Pt–Co layer assemblies

Furthermore, the influence of the layer configuration on the ORR activity was tested by using different deposition parameters, but with the same Pt loading. For example the catalyst is synthesized with 1, 2 or 4 layers of Co intertwined between the Pt layers. Moreover one catalyst with a decreasing Pt amount ($PtCo_E$) and one catalyst with an increasing Pt amount ($PtCo_D$) have been created, as it was investigated with Pt–C layers by Brault et al. [32]. Detailed descriptions of the catalyst shapes are summarized in Table 1. The thickness of each interrupting Co layer is 2 nm. The kinetic current of the ORR can be improved by a factor of 3.7–16 against pure Pt (Figs. 5 and 4). The lowest enhancement is achieved with 3 layers of Co. Interestingly j_{kin} increases by a factor of 10 when 2 layers of Pt are interrupted by one layer of Co ($PtCo_A$), far more than the Pt–Co sample which is intertwined by 4 layers of Co ($PtCo_C$) and 2 layers of Co ($PtCo_B$). The highest factor is gained when the thickness of the Pt layer is not constant in one sample. Decreasing the thickness of the Pt layer in the catalyst $PtCo_E$, j_{kin} is 16 times higher than the Pt standard and the onset potential is decreased significantly. This is quite interesting because in this case, most of the Pt is concentrated in the inner side of the catalyst compared to $PtCo_D$ where most of the Pt is concentrated in the outer side of the CL. Normally one would assume a higher current density would be found associated with a catalyst where Pt is concentrated in closer proximity to the oxygen containing solution.

Besides the fact that j_{kin} is higher with the Pt–Co catalysts it is obvious from the Tafel plots (Fig. 4b and Fig. 5b) that the Pt–Co samples are more active than pure Pt which is visible in the shifted Tafel plots. Normally the Tafel plot exhibits two different values, 2.3 RT/F at low overpotentials and 2*2.3 RT/F at higher overpotentials due to a change of the adsorption term [33]. In sulphuric acid the change in the Tafel slope is only small due to bisulfate adsorption [34,27]. According to Gasteiger et al. [27] we also calculated two values for the Tafel slope to determine the change in the Tafel slope for E higher and lower 0.85 V vs. NHE to get insights into the reaction mechanism. The curves of the Tafel plot and therefore the difference of the slope at low and high overpotentials do not change very much comparing Pt and Pt–Co samples indicating the reaction mechanism is not changing significantly. Only the Pt–Co sample with 1.5 nm Co exhibits a considerably reduced slope, with 60 mV dec^{-1} at low overpotentials, comparable to an optimal slope [27,35]. We calculated the transferred electrons by using the experimental derived B-Factor from the Koutecky Levich plot (E = 500 mV vs. NHE, RPM = 400, 900, 1600, 2500) and the Levich equation with previously reported theoretical data (D = 1.93 × 10^{-5} cm^2 s^{-1}, C_0 = 1.26 × 10^{-6} mol cm^{-3}, ν = 001009 cm^2 s^{-1}) [36,35]. Nearly 4 electrons take part in the oxygen reduction reaction with pure sputtered Pt (3,96). For $PtCo_C$ the number of transferred electrons is slightly diminished to 3,85. The widespread variety of ORR activities of the synthesized Pt–Co catalysts might have several reasons. Either more Co gets dissolved in the dissolution process so the real surface area is considerably larger or the electronic enhancement effect of Co on Pt is higher. It is to mention that in the work of Schwanitz [23] with a broadly similar synthesis process the complete solution of Co was not achieved after electrochemical treatment. This is in contrast to our synthesis method, where the entire Co is dissolved in the electrochemical cell. It has to be addressed that the GDE has to be preleached before assembling the MEA. This can be done in an electrolysis cell which is capable of applying higher currents. Entire leaching will be proven by ICP-AES measurements. By using a GDE rather than a catalyst coated membrane a poisoning of the membrane can be circumvented. However, SEM measurements showed a slight delamination of the plasma-deposited catalyst layer from the glassy carbon electrode after electrochemical RDE measurements with fast rotation speeds (3600 RPM) which was also seen in the diminished linear sweep voltammograms. Therefore stability issues have to be improved in future research.

3.2.4. PEM single cell tests

In order to investigate the realistic gas diffusion electrode behaviour the RDE technique is not suitable due to the fact that the oxygen flow is much higher, H^+ transfer is limiting, the current

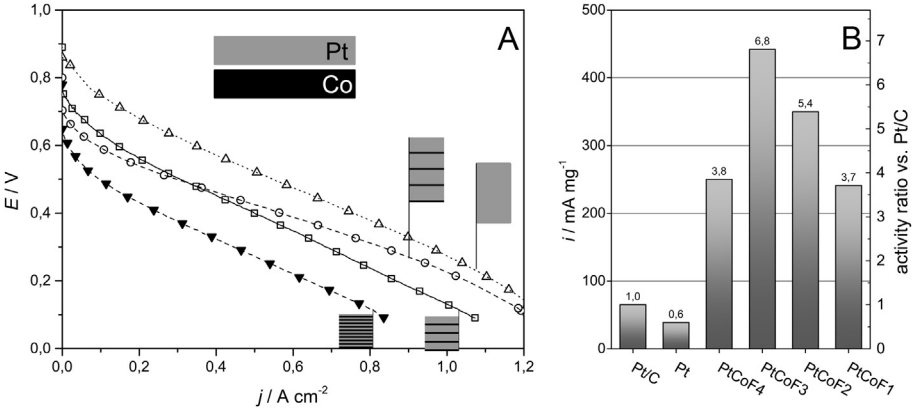

Fig. 6. PEM single cell tests at 346 K, 100% RH, H_2/air. A Single Cell PEM polarization curves with pure Pt (total Pt 0.7 mg cm^{-2})(···△···), $PtCo_{F1}$ (total Pt 0.12 mg cm^{-2}) (--○--), $PtCo_{F2}$ (total Pt 0.06 mg cm^{-2}), $PtCo_{F3}$ (total Pt 0.06 mg cm^{-2})(—□—), $PtCo_{F4}$ (total Pt 0.06 mg cm^{-2})(--▼--) and B mass activities and activity ratios vs. Pt/C at 350 mV (B).

distribution is inhomogeneous and higher current densities are possible in GDE. It is advisable to test the catalyst with a gas diffusion electrode half-cell test-method but there are only few prototypes available [30,37]. Nevertheless, the PEM single cell is an adequate technique to test the catalyst properties.

The Pt–Co MEA shows mass activities at 350 mV that are up to 7 times higher than the conventional MEA (Pt/C, screenprinted), Fig. 6. However, when Pt is sputtered only, the mass activity is even worse than that of Pt/C, especially at high Pt loadings. This can be assigned to mass transfer problems [38] and ohmic losses, which may result from the internal resistance of the electrode. By using the dual-magnetron sputter process these problems may be overcome. The polarization curves for $PtCo_{F1}$, $PtCo_{F3}$ and $PtCo_{F4}$ show similar voltage loss due to activation at low overpotentials. The ohmic loss stays nearly the same in all samples. $PtCo_{F1}$ was clearly observed to have a lower ohmic loss. It is possible that the internal resistance of this electrode is smaller. However, at higher current densities the mass transfer becomes limiting. The Pt loading in $PtCo_{F1}$ is twice of the value of the loading in $PtCo_{F2}$, but it shows a lower mass activity, indicating mass transfer problems. This is probably due to the higher thickness of the catalyst layer.

4. Conclusion

Mesoporous catalysts with significantly enhanced ORR activity are synthesized by alternating sputtering of Pt and Co. Therefore the Pt content of PEMFC catalysts can be significantly reduced retaining high performance of the fuel cell. By this new approach mass transfer problems, which normally occur in the thicker sputtered Pt catalysts are overcome. SEM images indicate that Co may be deposited at the grain boundaries of the formerly deposited Pt layer. This enables formation of mesopores that allow optimal gas diffusion in the catalyst layer. Epitaxially grown Pt–Co layers show a strong dependence of the electrochemical activity on the layer thickness. The optimal thickness at which the highest Pt mass activity was reached had a nominal value of 30.5 nm. Moreover, by varying the Pt layer thickness, the kinetic current was maximised in comparison to other samples with similar Pt loading. In half-cell tests it was shown that the best Co layer thickness was 2 nm. To summarize, the kinetic current was found to be increased by a factor of 16 in the RDE and the mass specific current in the PEM single cell is enhanced by a factor of 7.

Acknowledgement

The authors would like to thank the AiF (Arbeitsgemeinschaft industrieller Forschung) for funding the project (KF2591202SL1 and KF2046505SL1) and Dr. Jan Schaefer for EDX measurements.

References

[1] Y. Yamada, K. Miyamoto, T. Hayashi, Y. Iijima, N. Todoroki, T. Wadayama, Surf. Sci. 607 (2013) 54–60.
[2] C.S. Rao, D.M. Singh, R. Sekhar, J. Rangarajan, Int. J. Hydrogen Energy 36 (2011) 14805–14814.
[3] P. Mani, R. Srivastava, P. Strasser, J. Power Sources 196 (2011) 666–673.
[4] M.H. Lee, J.S. Do, J. Power Sources 188 (2009) 353–358.
[5] B.N. Popov, J. Power Sources 155 (2006) 253–263.
[6] M.K. Debe, A.K. Schmoeckel, G.D. Vernstrom, R. Atanasoski, J. Power Sources 161 (2006) 1002–1011.
[7] A. Rabis, P. Rodriguez, T.J. Schmidt, ACS Catal. 2 (2012) 864–890.
[8] V. Stamenkovic, B. Mun, M. Arenz, Nat. Mater. 6 (2007) 241–247.
[9] V.R. Stamenkovic, B. Fowler, B.S. Mun, G. Wang, P.N. Ross, C.A. Lucas, N.M. Markovic, Science 315 (2007) 493–497.
[10] V. Stamenkovic, B.S. Mun, K.J.J. Mayrhofer, P.N. Ross, N.M. Markovic, J. Rossmeisl, J. Greeley, J.K. Nörskov, Angew. Chem. Int. Ed. 45 (2006) 2897–2901.
[11] V.R. Stamenkovic, B.S. Mun, K.J.J. Mayrhofer, P.N. Ross, N.M. Markovic, J. Am. Chem. Soc. 6 (2006) 8813–8819.
[12] L. Dubau, M. Lopez-Haro, L. Castanheira, J. Durst, M. Chatenet, P. Bayle-Guillemaud, L. Guétaz, N. Caqué, E. Rossinot, F. Maillard, Appl. Catal. B: Environ. 142-143 (2013) 801–808.
[13] K. Mayrhofer, D. Strmcnik, B. Blizanac, V. Stamenkovic, M. Arenz, M. Markovic, Electrochimica Acta 53 (2008) 3181–3188.
[14] M. Nesselberger, S. Ashton, J.C. Meier, I. Katsounaros, K.J.J. Mayrhofer, M. Arenz, J. Am. Chem. Soc. 133 (2011) 17428–17433.
[15] A.B. Papandrew, R.W. Atkinson, G.a. Goenaga, S.S. Kocha, J.W. Zack, B.S. Pivovar, T.A. Zawodzinski, J. Electrochem. Soc. 160 (2013) F848–F852.
[16] M.K. Debe, J. Electrochem. Soc. 160 (2013) F522–F534.
[17] D. van der Vliet, C. Wang, D. Tripkovic, D. Strmcnik, X. Zhang, M. Debe, R. Atanasoski, N. Markovic, V. Stamenkovic, Nat. Mater. 11 (2012) 1051–1058.
[18] J. Kibsgaard, Y. Gorlin, Z. Chen, T. Jaramillo, J. Am. Chem. Soc. 134 (2012) 7758–7765.
[19] W. Liu, P. Rodriguez, L. Borchardt, A. Foelske, J. Yuan, A.-K. Herrmann, D. Geiger, Z. Zheng, S. Kaskel, N. Gaponik, R. Kötz, T.J. Schmidt, A. Eychmüller, Angew. Chem. Int. Ed. 52 (2013) 9849–9852.
[20] Z. Chen, M. Waje, W. Li, Y. Yan, Angew. Chem. 119 (2007) 4138–4141.
[21] T. Toda, H. Igarashi, H. Uchida, M. Watanabe, J. Electrochem. Soc. 146 (1999) 3750–3756.
[22] A. Bonakdarpour, K. Stevens, G.D. Vernstrom, R. Atanasoski, A.K. Schmoeckel, M.K. Debe, J.R. Dahn, Electrochimica Acta 53 (2007) 688–694.
[23] B. Schwanitz, Reduzierung der Platinbeladung und Imaging von Alterungsphaenomenen in der Polymerelektrolyt-Brennstoffzelle, 2012.
[24] S.H. Kang, Y.-E. Sung, W.H. Smyrl, J. Electrochem. Soc. 155 (2008) B1128–B1135.
[25] O. Himanen, T. Hottinen, S. Tuurala, Electrochem. Commun. 9 (5) (2007) 891–894.
[26] J. Zhang, PEM Fuel Cell Electrocatalysts and Catalyst Layers, Fundamentals and Applications, Springer Verlag, 2008.
[27] U. Paulus, T. Schmidt, H. Gasteiger, R. Behm, J. Electroanal. Chem. 495 (2001) 134–145.
[28] R.O Hayre, S.-J. Lee, S.-W. Cha, F. Prinz, J. Power Sources 109 (2) (2002) 483–493.
[29] S. Cha, W. Lee, J. Electrochem. Soc. 146 (1999) 4055–4060.
[30] C.M. Zalitis, D. Kramer, A.R. Kucernak, Phys. Chem. Chem. Phys. 15 (2013) 4329–4340.
[31] K. Kinoshita, J. Electrochem. Soc. 137 (1990) 845–848.
[32] H. Rabat, P. Brault, Fuel Cells 8 (2008) 81–86.
[33] U. Paulus, A. Wokaun, J. Phys. Chem. B 106 (16) (2002) 4181–4191.
[34] J.X. Wang, N.M. Markovic, R.R. Adzic, J. Phys. Chem. B 108 (13) (2004) 4127–4133.
[35] N.M. Markovic, H.A. Gasteiger, P.N. Ross, J. Phys. Chem. 99 (11) (1995) 3411–3415.
[36] V. Stamenkovic, T. Schmidt, P.N. Ross, N.M. Markovic, J. Phys. Chem. B 106 (2002) 11970–11979.
[37] T. Vidaković, M. Christov, K. Sundmacher, Electrochim. Acta 49 (2004) 2179–2187.
[38] M.D. Gasda, R. Teki, T.-M. Lu, N. Koratkar, G.A. Eisman, D. Gall, J. Electrochem. Soc. 156 (2009) B614–B619.